Charge Radius of Neutron-Deficient math xmlns="http://www.w3.org/1998/Math/MathML" display="inline">mrow>mmultiscripts>mrow>mi>Ni/mi>/mrow>mprescripts>/mprescripts>none>/none>mrow>mn>54/mn>/mrow>/mmultiscripts>/mrow>/math> and Symmetry Energy Constraints Using the Difference in Mirror Pair Charge Radii

Skyy V. Pineda, Kristian König, Dominic M. Rossi, B. Alex Brown, Anthony Incorvati, Jeremy Lantis, Kei Minamisono, Wilfried Nörtershäuser, Jorge Piekarewicz, Robert Powel, and Felix Sommer

Phys. Rev. Lett. **127**, 182503 — Published 29 October 2021

DOI: 10.1103/PhysRevLett.127.182503

Charge Radius of Neutron-deficient ^{54}Ni and Symmetry Energy Constraints Using the Difference in Mirror Pair Charge Radii

Skyy V. Pineda,[1,2,*] Kristian König,[1] Dominic M. Rossi,[3,4] B. Alex Brown,[1,5] Anthony Incorvati,[1,5] Jeremy Lantis,[1,2] Kei Minamisono,[1,5,†] Wilfried Nörtershäuser,[3] Jorge Piekarewicz,[6] Robert Powel,[1,5] and Felix Sommer[3]

[1]*National Superconducting Cyclotron Laboratory, Michigan State University, East Lansing, Michigan 48824, USA*
[2]*Department of Chemistry, Michigan State University, East Lansing, Michigan 48824, USA*
[3]*Institut für Kernphysik, Technische Universität Darmstadt, 64289 Darmstadt, Germany*
[4]*GSI Helmholtzzentrum für Schwerionenforschung mbH, Planckstr. 1, 64291 Darmstadt, Germany*
[5]*Department of Physics and Astronomy, Michigan State University, East Lansing, Michigan 48824, USA*
[6]*Department of Physics, Florida State University, Tallahassee, Florida 32306, USA*

(Dated: September 27, 2021)

The nuclear root-mean-square charge radius of ^{54}Ni was determined with collinear laser spectroscopy to be $R(^{54}\text{Ni}) = 3.737\,(3)$ fm. In conjunction with the known radius of the mirror nucleus ^{54}Fe, the difference of the charge radii was extracted as $\Delta R_{\text{ch}} = 0.049\,(4)$ fm. Based on the correlation between ΔR_{ch} and the slope of the symmetry energy at nuclear saturation density (L), we deduced $21 \leq L \leq 88\,\text{MeV}$. The present result is consistent with the L from the binary neutron star merger GW170817, favoring a soft neutron matter EOS, and barely consistent with the PREX-2 result within 1σ error bands. Our result indicates the neutron-skin thickness of ^{48}Ca as 0.15 - 0.21 fm.

Introduction — Knowledge of the slope of the symmetry energy L in the nuclear equation of state (EOS) is critical for the extrapolation to the higher densities [1] that are required to predict the properties of both super-heavy nuclei and neutron stars [2–4]. In the case of neutron stars, the "softness" or "stiffness" of the EOS has a direct link to the neutron star radius [5]. Note that a stiff EOS indicates that the pressure increases rapidly with increasing density. Conceptually, the symmetry energy is closely related to the difference between the energy per nucleon of pure neutron matter and symmetric nuclear matter. Given that symmetric nuclear matter saturates, L is proportional to the pressure of pure neutron matter at nuclear saturation density ρ_0 [6]. Different parameterizations of Skyrme energy density functionals show dramatic variations in the stiffness of the EOS [1], therefore making the extrapolations to higher densities uncertain. The stiffness of the EOS in the vicinity of ρ_0 is controlled by L, and although L cannot be directly determined through experiment, the neutron skin thickness ΔR_{np}, defined as the difference between root-mean-square charge radii of neutrons and protons, of neutron rich nuclei is strongly correlated to L [7, 8], which may then be used to set boundaries on its value [6].

The lead radius experiments PREX-1 [9] and PREX-2 [10] provide a direct probe of neutron densities via parity violating electron scattering. Given that the weak charge of the neutron is much larger than that of the proton, it paves an electroweak avenue to constrain the density dependence of the symmetry energy. Other electromagnetic methods involve a correlation between the electric dipole polarizability and the ΔR_{np} [11, 12]. Such measurements have been performed in ^{208}Pb [13, 14], ^{48}Ca [15], and in radioactive ^{68}Ni [16]. Besides terrestrial experiments, the binary neutron star merger GW170817 has placed important constraints on the EOS through the analysis of the tidal polarizability (or deformability) [17]. Various studies have aimed to translate the measurements on the neutron star merger into constraints on the EOS of dense neutron matter. However, whether the EOS is soft or stiff—which in turn translates into smaller or larger neutron star radii, respectively—is still under debate [17–26].

Another purely electromagnetic method to constrain L has been introduced in [6, 27], where the ΔR_{np} is deduced from the difference in charge radii between a mirror pair. Assuming perfect charge symmetry, the neutron radius of a given nucleus should be equal to the proton radius of the corresponding mirror nucleus. The ΔR_{np} can then be obtained from the difference ΔR_{ch} of the root-mean-square (rms) charge radii R_{ch} of mirror nuclei [6, 28] as $\Delta R_{\text{np}} = R_{\text{ch}}\left(^{A}_{Z}X_N\right) - R_{\text{ch}}\left(^{A}_{N}Y_Z\right) = \Delta R_{\text{ch}}$, where $A = N+Z$ is the mass number, and N and Z are the neutron and proton number, respectively. In reality, however, the charge symmetry is broken by the Coulomb interaction that pushes protons out relative to neutrons, leading to a weaker correlation between ΔR_{np} and ΔR_{ch}. It was shown that ΔR_{ch} is strongly correlated with $|N-Z| \times L$ even when $|N-Z|$ is small [6]. On the other hand, ΔR_{np} depends on both $|N-Z| \times L$ and the symmetry energy with the L dependence dominating at large $|N-Z|$ [6]. Such experiments provide a clean and largely model independent complement to the parity violating asymmetry experiments. In the present study, the mirror charge radii formalism is applied to the ^{54}Ni-^{54}Fe pair. The rms charge radius of ^{54}Ni was determined for the first time and then combined with the known radius of stable ^{54}Fe [29]. Although this pair has a smaller $|N-Z| = 2$ relative to our previous measurement on the ^{36}Ca-^{36}S mirror pair [30], the precise determination of the charge radius of ^{54}Ni provides a meaningful constraint on L,

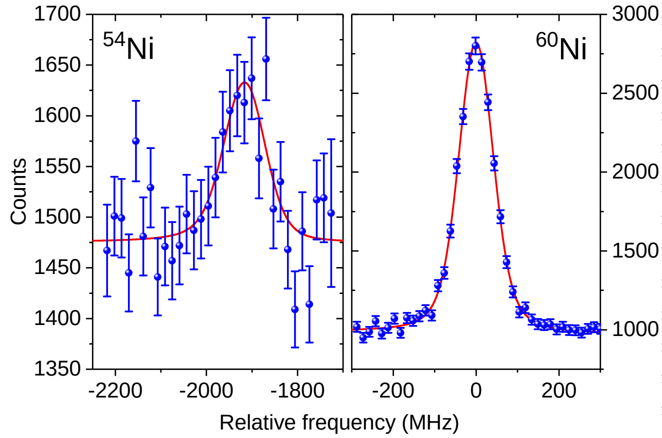

FIG. 1. Resonance spectra for ^{54}Ni (left) and ^{60}Ni (right) relative to the rest-frame transition frequency of ^{60}Ni. The solid line is the fit to the data.

with input from modern nuclear models.

Experiment — This experiment took place at the National Superconducting Cyclotron Laboratory at Michigan State University. A ^{58}Ni primary beam was impinged upon a beryllium target and the produced ^{54}Ni($I^{\pi} = 0^{+}$, $T_{1/2} = 114$ ms) beam was filtered out using the A1900 fragment separator. The isolated ^{54}Ni beam was then thermalized in a gas cell [31], extracted at an energy of 30 keV and transported to the BECOLA facility [32, 33]. A typical rate of Ni^{+} ions at the entrance of the BECOLA was 400/s. At BECOLA the Ni beam was captured, cooled and bunched in a radio frequency quadrupole (RFQ) ion trap [34]. The ion beam was extracted from the RFQ at an approximate energy of 29850 eV. Then the beam was neutralized in-flight in a charge-exchange cell (CEC) [35]. The typical neutralization efficiency was 50%, and the metastable $3d^9 4s\ ^3\mathrm{D}_3$ state was populated, which was estimated by a simulation to be 15% [36] of the total population. A small scanning potential (typically 50 V) was applied to the CEC to change the velocity of the incident ion beam and thus of the atom beam. This in turn Doppler-shifted the laser frequency in the rest frame of the atoms, and effectively scanned the laser frequency to measure the hyperfine spectrum. Ions in the metastable state were excited with 352-nm laser light to the $3d^9 4p\ ^3\mathrm{P}_2$ state, and fluorescence light was recorded as a function of the scanning voltage with a mirror-based fluorescence detection system[32, 37]. A background suppression factor of $2{\times}10^5$ was achieved by performing time-resolved fluorescence measurements with the bunched beam [33, 38, 39].

A Penning Ionization Gauge (PIG) ion source [36] was used to generate beams of stable ^{58,60}Ni isotopes, and spectroscopy was performed every 4-6 hours throughout the data taking time for ^{54}Ni. The resonance frequencies of ^{58,60}Ni were used as the reference for the extraction of the ^{54}Ni isotope shift as well as to determine the kinetic beam energy with 10^{-5} relative accuracy [40]. When changing between the isotopes, the laser frequency was adjusted to perform spectroscopy at the same beam energy. The applied laser frequencies were referenced against molecular iodine transition lines [41].

Experimental Results — The observed resonance line of ^{54}Ni is shown in Fig. 1 (left). A Voigt function with an exponential low-energy tail to describe the asymmetry caused by inelastic collisions with the sodium vapor [35] was used to fit the ^{54}Ni spectrum, and the fit result is shown as a solid line. The asymmetry parameter and the Lorentz width of the Voigt function were fixed to those obtained from the reference measurements on ^{58}Ni and ^{60}Ni. A typical spectrum of ^{60}Ni is shown in Fig. 1 (right) as an example of a stable isotope measurement.

The isotope shifts defined as $\delta\nu^{A,A'} = \nu^{A} - \nu^{A'}$ were extracted and summarized in Table I. The uncertainty is dominated by the statistical uncertainty of the ^{54}Ni resonance centroid (7.5 MHz). A discussion of the systematic uncertainty contributions is detailed in [42]. From the obtained isotope shifts, the differential mean square (ms) charge radius was extracted as $\delta\langle r^2\rangle^{A,A'} = (\delta\nu^{A,A'} - \mu^{A,A'}K_{\alpha})/F + \mu^{A,A'}\alpha$ [43] with the offset parameter α, the field-shift factor F, the offset-dependent mass-shift factor K_{α}, and $\mu^{A,A'} = (m_A - m_{A'})/\{(m_A + m_e)(m_{A'} + m_e)\}$, where m_A and $m_{A'}$ are the nuclear masses, and m_e is the electron mass. The F and K_{α} were separately determined [42] by the King-fit analysis [44] using re-measured isotope-shifts of the stable isotopes, and are listed in Tab. I for ^{58}Ni and ^{60}Ni as reference isotopes. Here, the offset parameter α was chosen to remove the correlation between the field- and mass-shift parameters in the linear regression. The obtained differential ms and the rms charge radii are also listed in Tab. I. The differential ms charge radii were used together with the known rms charge radii for reference isotopes to determine the rms charge radius of ^{54}Ni as $R(^{54}\mathrm{Ni}) = \{(R(^{A'}\mathrm{Ni}))^2 + \delta\langle r^2\rangle^{54,A'}\}^{1/2}$. The rms charge radii of ^{58}Ni, ^{60}Ni and ^{54}Fe were evaluated by combining tabulated values [29] for the Barrett radii $R_{k\alpha}$ from muonic spectroscopy and for the ratio of the radial moments V_2 from electron scattering, which yields

TABLE I. Isotope shift, atomic parameters, differential ms and rms charge radii of ^{54}Ni for $A' = 58$ and $A' = 60$ as the reference isotope are summarized.

	$A' = 58$	$A' = 60$
$\delta\nu^{54,A'}$ / MHz	-1410.4 (8.2)	-1919.7 (7.9)
α / u fm^2	417	388
K_{α} / GHz/u	929.8 (2.2)	954.0 (3.5)
F / MHz/fm^2	-767 (70)	-804 (66)
$\delta\langle r^2\rangle^{54,A'}$ / fm^2	-0.235 (29)	-0.522 (20)
$R(^{54}\mathrm{Ni})$ / fm	3.738 (4)	3.737 (3)

the model-independent rms charge radii $R_{\rm ch} = R_{k\alpha}/V_2$ as 3.7698 (16) fm, 3.8059 (17) fm and 3.6880 (17) fm, respectively. With the rms charge radii of ^{54}Fe the difference in mirror charge radii was determined to be $\Delta R_{\rm ch} = R(^{54}\mathrm{Ni}) - R(^{54}\mathrm{Fe}) = 0.049\,(4)$ fm.

Theoretical radii — Predictions were made for the difference in charge radii of ^{54}Ni and ^{54}Fe using the 48 Skryme energy-density functionals (EDF) [6] and the covariant density-functional (CODF) theory where a correlation between $\Delta R_{\rm ch}$ and L was also observed [28].

For the $A = 36$ mirror pair [30], it was found that the Skyrme results are sensitive to the isoscalar (IS) or the isoscalar plus isovector (IS+IV) forms of the spin-orbit potential. However, the present $A = 54$ pair turns out to be insensitive to the forms. The IS results is about 0.003 fm larger in $\Delta R_{\rm ch}$, which is negligible, and therefore we adapted the standard IS+IV form in this paper.

The Skyrme [6] and CODF [45] calculations include the relativistic spin-obit (RSO) correction to the charge radius [46], and were performed for spherical nuclei. It is known that the quadrupole correlations increase the rms radii when the saturation condition of isoscalar nuclear matter is taken into account [47]. In the present work, the quadrupole deformation effects were taken into account as a correction, which is discussed in the following.

The Bohr Hamiltonian starts with an expansion of the nuclear surface in terms of of its multipole degrees of freedom

$$R(\theta,\phi) = R_0\left[1+\sum_{\lambda,\mu}\alpha_{\lambda,\mu}Y_{\lambda,\mu}(\theta,\phi)\right], \qquad (1)$$

where R_0 is the radius of the nucleus when it has the spherical equilibrium shape, and $Y_{\lambda,\mu}$ is the spherical harmonic. The integrals of Eq. (1) involve $\beta^2 = \sum_{\lambda\geq 2}\sum_\mu \mid \alpha_{\lambda,\mu}\mid^2$. To order β^2, the volume integral of Eq. (1) is $I_0 = \{R_0^3(4\pi + 3\alpha_0\sqrt{4\pi} + 3\beta^2)\}/3$. Proton ($q = p$), neutron ($q = n$) and matter ($q = m$) distributions are distinguished by using R_{0q}, α_{0q} and β_q. For the matter density, if we impose the condition of saturation (that the average interior density remains constant), then the volume must be conserved, $I_0 = 4\pi R_{0m}^3/3$. This condition can be imposed by having

$$\alpha_{0m} = -\frac{\beta_m^2}{\sqrt{4\pi}}. \qquad (2)$$

To order β^2, the r^2 integral is $I_2 = \{R_0^5(4\pi + 5\alpha_0\sqrt{4\pi} + 10\beta^2)\}/5$. With the condition of volume conservation from Eq. (2), the matter ms radius is

$$\left\langle r^2\right\rangle_m = \frac{I_2}{I_0} = \left\langle r^2\right\rangle_{0m}\left[1+\frac{5}{4\pi}\beta_m^2\right], \qquad (3)$$

where $\left\langle r^2\right\rangle_{0m} = 3R_{0m}^2/5$ is the ms radius with no deformation. If $\beta_p = \beta_n = \beta_m$, then we can use Eq. (3) for protons. But if $\beta_p \neq \beta_n$, one must make some assumptions about the α_0 term. If we take $\alpha_{0p} = \alpha_{0n} = \alpha_{0m}$ for the volume correction, then

$$\begin{aligned}\left\langle r^2\right\rangle_p &= \left\langle r^2\right\rangle_{0p}\left[1+\frac{2\alpha_{0p}}{\sqrt{4\pi}}+\frac{7}{4\pi}\beta_p^2\right]\\ &= \left\langle r^2\right\rangle_{0p}\left[1-\frac{2}{4\pi}\beta_m^2+\frac{7}{4\pi}\beta_p^2\right]. \end{aligned} \qquad (4)$$

For $\lambda = 2$, the β_p are related to the $B(E2,\uparrow)_p$ for 0^+ to 2^+ (in units of e^2) by $\beta_p = 4\pi\sqrt{B(E2,\uparrow)_p}/(5a_q\left\langle r^2\right\rangle_{0p})$, where $a_q = Z$ for protons. For β_n and β_m we have equivalent expressions with $a_q = N$ and A. The calculated $B(E2,\uparrow)_p$ can be compared to experimental results, whereas $B(E2,\uparrow)_n$ and $B(E2,\uparrow)_m$ are much less known. We calculate the matrix elements $M_q = \sqrt{B(E2,\uparrow)_q}$ from full-basis configuration interaction calculations in the fp shell model space with the GFPX1A [48] and KB3G [49] Hamiltonians. The $E2$ matrix elements calculated in the fp model space are denoted by A_q. The radial matrix elements were calculated with harmonic-oscillator radial wavefunctions with $\hbar\omega = 45A^{\frac{-1}{3}} - 25A^{\frac{-2}{3}}$ [50]. The full matrix element is obtained with "effective charges" e_q that arise from the coupling of the fp nucleons to the $2\hbar\omega$ giant quadrupole resonances as $M_p = A_pe_p + A_ne_n$. From mirror symmetry we have $A_p(^{54}\mathrm{Ni}) = A_n(^{54}\mathrm{Fe})$ and $A_n(^{54}\mathrm{Ni}) = A_p(^{54}\mathrm{Fe})$. We can write M_p in terms of its isoscalar (0) and isovector (1) contributions $M_p = M_0 + M_1 = A_0e_0 + A_1e_1$ where $A_0 = (A_p + A_n)/2$, $A_1 = (A_p - A_n)/2$, $e_0 = e_p + e_n$ and $e_1 = e_p - e_n$. $E2$ transitions are dominated by A_0 and thus the isoscalar effective charge is well established, $e_0 = 2.0(1)$ by systematic comparison to data [51]. The $[A_p, A_n, A_0, A_1]$ for ^{54}Fe are [16.5, 7.9, 12.2, 4.3] and [14.8, 6.0, 10.4, 4.4] fm^2 for GPFX1A and KB3G, respectively. For ^{54}Fe, $M_p > M_n$ since the wavefunctions for the 0^+ and 2^+ states are dominated (about 50%) by the configuration with two proton $0f_{7/2}$ holes in a ^{56}Ni closed-shell configuration.

The main contribution to the radius shift is from the M_1 term. The isoscalar effective charge e_1 has been determined by comparing $E2$ transition in the mirror nuclei ^{51}Fe and ^{51}Mn [52]. The result obtained in [52] with KB3G is $A_1 = 5.86$ fm^2, and $e_1 = 1 - 2e^{(1)}_{\rm pol} = 0.37$ ($e^{(1)}_{\rm pol}$ is the parameter used in [52]). We have reanalyzed those data with GPFX1A and obtain $A_1 = 4.56$ fm^2 and $e_1 = 0.47$ with the harmonic-oscillator parameter used in [52], and with our parameter we obtain $A_1 = 4.85$ fm and $e_1 = 0.44$. The e_1 is reduced from its free-nucleon value of one, due to coupling of the fp nucleons to the isovector giant-quadrupole resonance. Based on these results we adopt a value and uncertainty of $e_1 = 0.44(10)$, resulting in $e_p = 1.22$ and $e_n = 0.78$.

The results for ^{54}Fe are $B(E2) = 690(90)$ and 630(80) e^2 fm^4 for GPFX1A and KB3G, respectively, to be compared to the experimental value of 640(23) e^2 fm^4 [53].

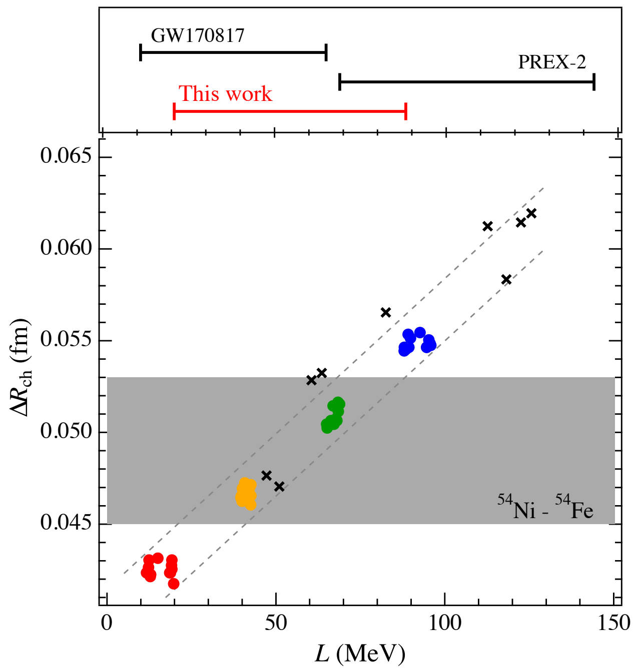

FIG. 2. $\Delta R_{\rm ch}$ as a function of L at ρ_0. The experimental result is shown as a horizontal gray band. The solid circles are results of Skyrme EDF and the crosses are for the CODF calculations. The dashed lines indicate theoretical error bounds. The upper figure shows comparison with the GW170817 and the PREX-2.

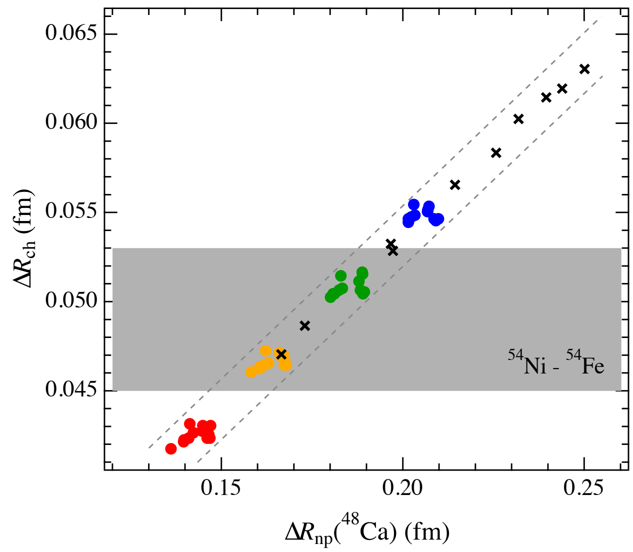

FIG. 3. "Data-to-data" relation between $\Delta R_{\rm ch}$ and $\Delta R_{\rm pn}(^{48}\mathrm{Ca})$. The same marks and color coding are used as Fig. 2.

The theoretical errors are dominated by the error in e_0. For a given value of M_1, we can use the experimental $M_p(\exp) = 25.3(5)$ e fm^2 [53] to constrain M_0 by $M_0 = M_p(\exp) - M_1$. The results for the ^{54}Fe β values are $[\beta_p, \beta_n, \beta_m] = [0.186(4), 0.147(7), 0.166(5)]$. The results for ^{54}Ni are 460(40) e^2 fm^4 and [0.147(7), 0.186(4), 0.166(5)]. The difference in these results between GPFX1A and KB3G is very small since the A_1 values are almost the same. The predicted $B(E2)$ for ^{54}Ni should be verified experimentally. The resulting contribution to $\Delta R_{\rm ch}$ is -0.0131(17) fm. The error in $\Delta R_{\rm ch}$ is dominated by the error e_1.

The quadrupole correlations are explicitly contained in the CHFB+5DCH calculations using the D1S Hamiltonian given in [54, 55]. They obtain $\Delta R_{\rm ch}(\mathrm{def}) = 0.058$ fm that goes with $L = 22.3$ MeV [45] for D1S. Their $B(E2)$ values are 1310 and 1580 e^2 fm^2 for ^{54}Fe and ^{54}Ni, respectively. This does not agree with experiment or the shell-model calculations, presumably because the ^{56}Ni core is too soft compared to experiment and the shell model.

Discussion — The resulting quadrupole correction for $\Delta R_{\rm ch}$ is added to the Skyrme and CODF calculations performed in the spherical basis. The results are shown in Fig. 2 by the colored points. The color indicates the neutron skin of ^{208}Pb: 0.12 fm (red), 0.16 fm (orange), 0.20 fm (green), and 0.24 fm (blue) for Skyrme calculations. The results of the CODF calculations are shown in crosses. The theoretical uncertainties in the correction for $\Delta R_{\rm ch}$ are shown using dashed lines.

The Skyrme and CODF calculations show consistent agreement in the correlation between $\Delta R_{\rm ch}$ and L. In comparison to these calculations, the experimental one-sigma error band shown in Fig. 2 in gray implies a value of L in the range of 21-88 MeV. In the top panel of Fig. 2 we compare the present result with the range for L of 11-65 MeV deduced from GW170817 [56], to which our result is consistent, suggesting a relatively soft neutron matter EOS. The present result is also compared against the recent PREX-2 result of $\Delta R_{\rm np} = 0.283\,(71)$ fm [10] that implies $L = 106\,(37)$ MeV [57]. Our result is barely consistent within 1σ error bands with the PREX-2, which indicates rather stiff EOS. It is noted that our previous results on the mirror pair ^{36}Ca-^{36}S indicates the range of $L =$ 5-70 MeV [30], which is consistent with the present results. However, the $A = 36$ result does not include the quadrupole correlation and has an ambiguity in the form of spin orbit force. The correction for the quadrupole correlation is expected to be small, and once the experimental $B(E2)$ for the $A = 36$ pair become available, the range from the $A = 36$ will be updated. In order to make the comparison on the same footing, the $A = 36$ result is not shown in Fig. 2.

Finally the correlation between $\Delta R_{\rm ch}$ and $\Delta R_{\rm np}(^{48}\mathrm{Ca})$ is shown in Fig. 3. Our $\Delta R_{\rm ch}$ restricts the $\Delta R_{\rm np}(^{48}\mathrm{Ca})$ to the interval of $0.15-0.21$ fm. The connection to ^{48}Ca is timely given that the Calcium Radius EXperiment (CREX) has been completed [58], where experimental error of about ± 0.02 fm is expected, which is comparable to the error obtained here. It is of particular interest whether CREX will confirm the soft EOS or reveal a larger ΔR_{np} as the PREX-2.

Summary — The ΔR_{ch} between mirror nuclei ^{54}Ni-^{54}Fe was evaluated, and compared with the Skyrme EDFs and the CODF theories. The ΔR_{ch} and L correlation implies a range of $L = 21$-88 MeV, and is consistent with the L from GW170817 and our previous result in the ^{36}Ca-^{36}S pair, suggesting a soft neutron matter EOS. Our result is barely consistent within 1σ error bands with the PREX-2 that indicates a stiff EOS. The present ΔR_{ch} also predicts the $\Delta R_{\mathrm{np}}(^{48}\mathrm{Ca})$ as 0.15–0.21 fm. More data on the mirror charge radii in different mass regions as well as theoretical studies for the quadrupole correlations are required to properly assess the model dependence and to set tighter limits on the L.

Acknowledgements This work is support in part by the National Science Foundation grant No. PHY-15-65546 and by the U.S. Department of Energy Office of Science, Office of Nuclear Physics under Award DE-FG02-92ER40750, and by the Deutsche Forschungsgemeinschaft (DFG, German Research Foundation) - Project-ID 279384907 - SFB 1245. We thank Nathalie Pillet for providing the CHFB+5DCH calculation results for ^{54}Ni and ^{54}Fe.

---

* pineda@frib.msu.edu
† minamiso@nscl.msu.edu

[1] B. Alex Brown, Neutron radii in nuclei and the neutron equation of state, Physical Review Letters **85**, 5296 (2000).

[2] C. J. Horowitz and J. Piekarewicz, Neutron star structure and the neutron radius of ^{208}Pb, Phys. Rev. Lett. **86**, 5647 (2001).

[3] A. W. Steiner, J. M. Lattimer, and E. F. Brown, The neutron star mass-radius relation and the equation of state of dense matter, Astrophysics **765**, L5 (2013).

[4] D. Steppenbeck, S. Takeuchi, N. Aoi, P. Doornenbal, M. Matsushita, H. Wang, H. Baba, N. Fukuda, S. Go, M. Honma, J. Lee, K. Matsui, S. Michimasa, T. Motobayashi, D. Nishimura, T. Otsuka, H. Sakurai, Y. Shiga, P.-A. Söderström, T. Sumikama, H. Suzuki, R. Taniuchi, Y. Utsuno, J. J. Valiente-Dobón, and K. Yoneda, Nature **502**, 207 (2013).

[5] J. M. Lattimer and M. Prakash, Neutron Star Observations: Prognosis for Equation of State Constraints, Phys. Rept. **442**, 109 (2007).

[6] B. A. Brown, Mirror charge radii and the neutron equation of state, Physical Review Letters **119**, 122502 (2017).

[7] X. Roca-Maza, M. Centelles, X. Viñas, and M. Warda, Neutron skin of ^{208}Pb, nuclear symmetry energy, and the parity radius experiment, Phys. Rev. Lett. **106**, 252501 (2011).

[8] P.-G. Reinhard and W. Nazarewicz, Nuclear charge and neutron radii and nuclear matter: Trend analysis in skyrme density-functional-theory approach, Physical Review C **93**, 051303(R) (2016).

[9] S. Abrahamyan *et al.* (PREX Collaboration), Measurement of the neutron radius of ^{208}Pb through parity violation in electron scattering, Physical Review Letters **108**, 112502 (2012).

[10] D. Adhikari *et al.*, Accurate determination of the neutron skin thickness of ^{208}Pb through parity-violation in electron scattering, Phys. Rev. Lett. **126**, 172502 (2021).

[11] P.-G. Reinhard and W. Nazarewicz, Information content of a new observable: The case of the nuclear neutron skin, Phys. Rev. C **81**, 051303(R) (2010).

[12] J. Piekarewicz, Pygmy resonances and neutron skins, Physical Review C **83**, 034319 (2011).

[13] A. Tamii, I. Poltoratska, P. von Neumann-Cosel, Y. Fujita, T. Adachi, C. A. Bertulani, J. Carter, M. Dozono, H. Fujita, K. Fujita, *et al.*, Complete electric dipole response and the neutron skin in ^{208}Pb, Phys. Rev. Lett. **107**, 062502 (2011).

[14] X. Roca-Maza, M. Brenna, G. Colò, M. Centelles, X. Viñas, B. K. Agrawal, N. Paar, D. Vretenar, and J. Piekarewicz, Electric dipole polarizability in ^{208}pb: Insights from the droplet model, Physical Review C **88**, 024316 (2013).

[15] J. Birkhan *et al.*, Electric dipole polarizability of ^{48}Ca and implications for the neutron skin, Phys. Rev. Lett. **118**, 252501 (2017).

[16] D. M. Rossi, P. Adrich, F. Aksouh, H. Alvarez-Pol, T. Aumann, J. Benlliure, M. Böhmer, K. Boretzky, E. Casarejos, M. Chartier, A. Chatillon, D. Cortina-Gil, U. Datta Pramanik, H. Emling, O. Ershova, B. Fernandez-Dominguez, H. Geissel, M. Gorska, M. Heil, H. T. Johansson, A. Junghans, A. Kelic-Heil, O. Kiselev, A. Klimkiewicz, J. V. Kratz, R. Krücken, N. Kurz, M. Labiche, T. Le Bleis, R. Lemmon, Y. A. Litvinov, K. Mahata, P. Maierbeck, A. Movsesyan, T. Nilsson, C. Nociforo, R. Palit, S. Paschalis, R. Plag, R. Reifarth, D. Savran, H. Scheit, H. Simon, K. Sümmerer, A. Wagner, W. Waluś, H. Weick, and M. Winkler, Measurment of the dipole polarizability of the unstable neutron-rich nucleus ^{68}Ni, Physical Review Letters **111**, 242503 (2013).

[17] B. P. Abbott *et al.* (The LIGO Scientific Collaboration and the Virgo Collaboration), GW170817: Measurements of neutron star radii and equation of state, Physical Review Letters **121**, 161101 (2018).

[18] B. P. Abbott *et al.* (the LIGO Scientific Collaboration and Virgo Collaboration), GW170817: Observation of gravitational waves from a binary neutron star inspiral, Physical Review Letters **119**, 161101 (2017).

[19] F. J. Fattoyev, J. Piekarewicz, and C. J. Horowitz, Neutron skins and neutron stars in the multi-messenger era, Phys. Rev. Lett. **120**, 172702 (2018).

[20] I. Tews, J. Margueron, and S. Reddy, Critical examination of constraints on the equation of state of dense matter obtained from GW170817, Phys. Rev. **C98**, 045804 (2018).

[21] M. Tsang, W. Lynch, P. Danielewicz, and C. Tsang, Symmetry energy constraints from GW170817 and laboratory experiments, Physics Letters B **795**, 533 (2019).

[22] Y. Zhang, M. Liu, C.-J. Xia, Z. Li, and S. K. Biswal, Constraints on the symmetry energy and its associated parameters from nuclei to neutron stars, Physical Review C **101**, 034303 (2020).

[23] H. Shen, F. Ji, J. Hu, and K. Sumiyoshi, Effects of symmetry energy on the equation of state for simulations of core-collapse supernovae and neutron-star mergers, The Astrophysical Journal **891** (2020).
[24] J. Hu, S. Bao, Y. Zhang, K. Nakazato, K. Sumiyoshi, and H. Shen, .
[25] Y. Li, H. Chen, D. Wen, and J. Zhang, Constraining the nuclear symmetry energy and properties of the neutron star from GW170817 by bayesian analysis, The European Physical Journal A **57**, 1 (2021).
[26] J. Estee *et al.* (SπRIT Collaboration), Probing the symmetry energy with the spectral pion ratio, Phys. Rev. Lett. **126**, 162701 (2021).
[27] N. Wang and T. Li, Shell and isospin effects in nuclear charge radii, Phys. Rev. C **88**, 011301(R) (2013).
[28] J. Yang and J. Piekarewicz, Difference in proton radii of mirror nuclei as a possible surrogate for the neutron skin, Phys. Rev. C **97**, 014314 (2018).
[29] G. Fricke and K. Heilig, *Nuclear Charge Radii* (Springer, Berlin Heidelberg, 2004).
[30] B. A. Brown, K. Minamisono, J. Piekarewicz, H. Hergert, D. Garand, A. Klose, K. König, J. D. Lantis, Y. Liu, B. Maaß, A. J. Miller, W. Nörtershäuser, S. V. Pineda, R. C. Powel, D. M. Rossi, F. Sommer, C. Sumithrarachchi, A. Teigelhöfer, J. Watkins, and R. Wirth, Implications of the ^{36}Ca-^{36}S and ^{38}Ca-^{38}Ar difference in mirror charge radii on the neutron matter equation of state, Physical Review Research **2**, 022035(R) (2020).
[31] C. Sumithrarachchi, D. Morrissey, S. Schwarz, K. Lund, G. Bollen, R. Ringle, G. Savard, and A. Villari, Beam thermalization in a large gas catcher, Nuclear Instruments and Methods in Physics Research Section B: Beam Interactions with Materials and Atoms **463**, 305 (2020).
[32] K. Minamisono, P. F. Mantica, A. Klose, S. Vinnikova, A. Schneider, B. Johnson, and B. R. Barquest, Commissioning of the collinear laser spectroscopy system in the becola facility at nscl, Nuclear Instruments and Methods in Physics Research A **709**, 85 (2013).
[33] D. M. Rossi, K. Minamisono, B. R. Barquest, G. Bollen, K. Cooper, M. Davis, K. Hammerton, M. Hughes, P. F. Mantica, D. J. Morrissey, R. Ringle, J. A. Rodriguez, C. A. Ryder, S. Schwarz, R. Strum, C. Sumithrarachchi, D. Tarazona, and S. Zhao, A field programmable gate array-based time-resolved scaler for collinear laser spectroscopy with bunched radioactive potassium beams, Review of Scientific Instruments **85**, 093503 (2014).
[34] B. R. Barquest, G. Bollen, P. F. Mantica, K. Minamisono, R. Ringle, and S. Schwarz, Rfq beam cooler and buncher for collinear laser spectroscopy of rare isotopes, Nucl. Instrum. Methods Phys. Res. A **866**, 18 (2017).
[35] A. Klose, Tests of atomic charge-exchange cells for collinear laser spectroscopy, Nuclear Instruments and Methods in Physics Research Section A: Accelerators, Spectrometers, Detectors and Associated Equipment **678**, 114 (2012).
[36] C. Ryder, K. Minamisono, H. Asberry, B. Isherwood, P. Mantica, A. Miller, D. Rossi, and R. Strum, Population distribution subsequent to charge exchange of 29.85 kev ni$^+$ on sodium vapor, Spectrochimica Acta Part B: Atomic Spectroscopy **113**, 16 (2015).
[37] B. Maaß, K. König, J. Krämer, A. J. Miller, K. Minamisono, W. Nörtershäuser, and F. Sommer, A 4π fluorescence detection region for collinear laser spectroscopy, arXiv:2007.02658 [physics.ins-det].
[38] P. Campbell, H. L. Thayer, J. Billowes, P. Dendooven, K. T. Flanagan, D. H. Forest, J. A. R. Griffith, J. Huikari, A. Jokinen, R. Moore, A. Nieminen, G. Tungate, S. Zemlyanoi, and J.Äystö, Laser spectroscopy of cooled zirconium fission fragments, Phys. Rev. Lett. **89**, 082501 (2002).
[39] A. Nieminen, P. Campbell, J. Billowes, D. H. Forest, J. A. R. Griffith, J. Huikari, A. Jokinen, I. D. Moore, R. Moore, G. Tungate, and J. Äystö, On-line ion cooling and bunhing for collinear laser spectroscopy, Physical Review Letters **88**, 094801 (2002).
[40] K. König, K. Minamisono, J. Lantis, S. Pineda, and R. Powel, Beam energy determination via collinear laser spectroscopy, Physical Review A **103**, 032806 (2021).
[41] R. Powel, Appl. Phys. B **in press** (2021).
[42] K. König, F. Sommer, J. Lantis, K. Minamisono, W. Nörtershäuser, S. Pineda, and R. Powel, Isotope-shift measurements and king-fit analysis in nickel isotopes, Physical Review C **103**, 054305 (2021).
[43] M. Hammen, W. Nörtershäuser, D. L. Balabanski, M. L. Bissell, K. Blaum, I. Budinčević, B. Cheal, K. T. Flanagan, N. Frömmgen, G. Georgiev, C. Geppert, M. Kowalska, K. Kreim, A. Krieger, W. Nazarewicz, R. Neugart, G. Neyens, J. Papuga, P.-G. Reinhard, M. M. Rajabali, S. Schmidt, and D. T. Yordanov, From calcium to cadmium: Testing the pairing functional through charge radii measurements of $^{100-130}$cd, Physical Review Letters **121**, 102501 (2018).
[44] W. H. King, *Isotope Shifts in Atomic Spectra, 1st edn.* (Springer Science+Business Media, New York, 1984).
[45] J.-P. Delaroche, M. Girod, J. Libert, H. Goutte, S. Hilaire, S. Peru, N. Pillet, and G. F. Bertsch, Structure of even-even nuclei using a mapped collective hamiltonian and the d1s gogny interaction, Phys. Rev. C **81**, 014303 (2010).
[46] C. J. Horowitz and J. Piekarewicz, Impact of spin-orbit currents on the electroweak skin of neutron-rich nuclei, Phys. Rev. C **86**, 045503 (2012).
[47] G. F. Bertsch, **55**, 248 (2019).
[48] M. Honma, T. Otsuka, B. Brown, and T. Mizusaki, Shell-model description of neutron-rich pf-shell nuclei with a new effective interaction gxpf1, Euro. Phys. J. A **25, s01**, 499 (2005).
[49] A. Poves, J. Sanchez-Solano, E. Caurier, and F. Nowacki, Shell model study of the isobaric chains $a = 50$, $a = 51$ and $a = 52$, Nucl. Phys. A **694**, 157 (2001).
[50] J. Blomqvist and A. Molinari, Collective 0^- vibrations in even spherical nuclei with tensor forces, Nucl. Phys. A **106**, 545 (1968).
[51] M. Honma, T. Otsuka, B. A. Brown, and T. Mizusaki, New effective interaction for pf-shell nuclei and its implications for the stability of the $N = Z = 28$ closed core, Phys. Rev. C **69**, 034335 (2004).
[52] R. du Rietz, J. Ekman, D. Rudolph, C. Fahlander, A. Dewald, O. Möller, B. Saha, M. Axiotis, M. A. Bentley, C. Chandler, G. de Angelis, F. DellaVedova, A. Gadea, G. Hammond, S. M. Lenzi, N. Marginean, D. R. Napoli, M. Nespolo, C. Rusu, and D. Tonev, Effective charges in the fp shell, Phys. Rev. Lett. **93**, 222501 (2004).
[53] K. L. Yurkewicz, D. Bazin, B. A. Brown, C. M. Campbell, J. A. Church, D. C. Dinca, A. Gade, T. Glasmacher, M. Honma, T. Mizusaki, W. F. Mueller, H. Olliver, T. Otsuka, L. A. Riley, and J. R. Terry, Nuclear

structure in the vicinity of $N = Z = 28$ ^{56}Ni, Phys. Rev. C **70**, 054319 (2004).

[54] J. Decharge and D. Gogny, Hartree-fock-bogolyubov calculations with the $d1$ effective interaction on spherical nuclei, Phys. Rev. C **21**, 1568 (1980).

[55] J.-F. Berger, M. Girod, and D. Gogny, Time-dependent quantum collective dynamics applied to nuclear fission, Comput. Phys. Commun. **63**, 365 (1991).

[56] C. A. Raithel and F. Özel, Measurement of the nuclear symmetry energy parameters from gravitational-wave events, Astrophys. J. **885**, 121 (2019).

[57] B. T. Reed, F. J. Fattoyev, C. J. Horowitz, and J. Piekarewicz, Implications of PREX-II on the equation of state of neutron-rich matter, Phys. Rev. Lett. **126**, 172503 (2021).

[58] CREX: Parity violating measurement of the weak charge distribution of ^{48}Ca, hallaweb.jlab.org/parity/prex/c-rex2013_v7.pdf.